Diffusion of acetylene inside Na-Y zeolite: Molecular dynamics simulation studies

Siddharth Gautam, S. Mitra, R. Mukhopadhyay,* and S. L. Chaplot
[1]*Solid State Physics Division, Bhabha Atomic Research Centre, Mumbai 400 085, India*
(Received 20 April 2006; published 3 October 2006)

Dynamics of acetylene molecules adsorbed in Na-Y zeolite cages is investigated using molecular dynamics simulation. The translational motion of the acetylene molecules is shown to involve three different time scales. "Free particle" type diffusion is observed in short time and small length scale. At long time and large length scale, center of mass motion of acetylene is determined by the zeolitic pore topology. Rotational motion of the acetylene is found to be very fast. Detailed analysis of the intermediate scattering function corresponding to the rotational motion showed large-angle jumps that could be described by an *m*-diffusion model.

DOI: 10.1103/PhysRevE.74.041202 PACS number(s): 51.20.+d, 02.70.−c, 51.90.+r, 66.20.+d

I. INTRODUCTION

Zeolites are a group of hydrated microporous crystalline aluminosilicates containing exchangeable cations from group 1A and 2A elements. They are useful in a number of industrial processes due to their characteristic properties like low density, high void volume in the form of cages, selective sorption, high stability over a large range of temperatures, and their catalytic properties. Because of their property of selective adsorption, zeolites can be used as molecular sieves for the purification of air. They have been widely used in separating nitrogen and oxygen from air as also for removing water from natural gases. Zeolites offer a wide range of catalytic applications especially in the petrochemical industry because of their acid strength and shape selectivity [1,2]. Zeolites have been under intense investigation due to their usefulness in a variety of applications [3–9]. An understanding of the molecular sieving property as also that of catalytic properties of the zeolites requires an understanding of diffusivity of the adsorbed molecules. This depends upon a number of factors like the shape of the molecule, pore characteristics, the volume of the cages, the molecule zeolite interaction, and temperature. A diffusion anomaly as a function of molecular length in hydrocarbons adsorbed in Na-Y zeolite was reported earlier [9]. NMR [10,11] and quasi elastic neutron scattering (QENS) [12,13] have been used to study molecular motions. MD simulation is a useful tool to study molecular motion [14,15], which not only provides insight on the details of the possible different types of motion but also does not suffer limitations of the experimental setup. Earlier we reported on a QENS study of the dynamics of acetylene molecules adsorbed in Na-Y zeolite cages that showed that the translational motion of acetylene molecules could be described by the Hall and Ross model [16] in which the molecules move through discrete jumps with a Gaussian distribution of jump lengths. To gain deeper insight into the dynamics of acetylene in Na-Y zeolite, we report in this paper on molecular dynamics (MD) simulations and compare the results with those obtained by the earlier QENS technique [17].

*Corresponding author; email address: mukhop@apsara.barc.ernet.in

II. SIMULATION DETAILS

A widely used zeolite is the Na-Y zeolite, which has especially large cavities called supercages. Moreover it is known to be highly organophillic because of its high Si/Al ratio (more than 2.5). These supercages have a diameter of 11.8 Å and are interconnected to each other in a tetrahedral manner through 12 membered oxygen rings with a diameter of 7.8 Å [18]. MD simulation studies were carried out on a cubic cell of length 24.8536 Å. Si/Al ratio taken was ∞. Although the effect of extra framework cations is significant for adsorption phenomena [19], but for self-diffusivity of the adsorbed species, the effect is only marginal [9]. Therefore, we used extra framework cation free zeolite for our simulation.

It is known that both self- and collective diffusivities strongly depend on the loading of the hydrocarbons inside zeolitic cages. Simulation [20] and experiments [21,22] have shown this. Our aim in this paper is to investigate the details of various time correlation functions with a loading at which our earlier experiment [17] was performed. Since the experiment was performed on samples with saturation loading which amounts to six molecule per zeolitic cage, the same concentration is used for the simulation.

Acetylene molecules were considered to be rigid. Positions of zeolitic atoms were held fixed in the simulation. Equations of motion were solved using a leapfrog form of the Verlet algorithm in microcanonical ensemble [14]. Cubic periodic boundary conditions were used and all molecular interactions at a distance greater than 12.0 Å were neglected for being insignificant. Rotational motion was monitored by following the change in the orientations of a unit vector along the molecular axis [14].

The interaction between the guest-guest as well as the guest-zeolite molecules was modeled by the Lennard-Jones potential given by:

$$\Phi(r_{ij}) = 4\varepsilon_{ij}\left[\left(\frac{\sigma_{ij}}{r_{ij}}\right)^{12} - \left(\frac{\sigma_{ij}}{r_{ij}}\right)^{6}\right], \quad (1)$$

where ε_{ij} is the well-depth, σ_{ij} is the diameter, and r_{ij} is the distance between the interacting atoms i and j. Acetylene molecules were modeled with a united atom model where the acetylene molecule is assumed to be a linear one with two CH sites separated by a distance of 1.21 Å. As the bulkier

TABLE I. Potential parameters for acetylene-acetylene and acetylene-zeolite interaction [24].

Interaction	σ(Å)	$\epsilon(K)$
CH-CH	3.800	57.879
CH-O	3.173	46.316

oxygens surround the Si and Al atoms, the close approach of guest to Si and Al atoms is not possible. Therefore short-range interactions are included between the guest and oxygens only [23]. The potential parameters were taken from the literature [9,24] and are listed in Table I. A calculation time step of 0.6 fs yielded good energy conservation. Equilibration was performed over a duration of 300 ps, during which velocities were scaled at every step to obtain the desired temperature of 300 K. This was followed by a production run for 1.3 ns during which configurations were stored at intervals of 0.02 ps for translational motion and 0.002 ps for rotational motion and averages for various quantities were calculated from them.

III. RESULTS AND DISCUSSION

In the case of molecular systems, different kinds of stochastic motions namely translations and rotations are present simultaneously. As we shall see later, the present MD simulation shows that the rotational motion of acetylene is much faster than the translational motion. Therefore we assume that these motions are dynamically independent and can be analyzed separately.

A. Translational motion

In a molecular dynamics simulation, diffusion coefficient for translational motion, D, can be obtained from the mean square displacement of molecules using Einstein's relation:

$$2tD = \frac{1}{N_t}\langle|\mathbf{r}(t+t_0) - \mathbf{r}(t_0)|^2\rangle, \tag{2}$$

where $\mathbf{r}$ is the position vector of the center of mass of the molecule, N_t is the number of degrees of freedom associated with translational motion (in the present case $N_t=3$) and $\langle\rangle$ denotes ensemble average. The diffusion coefficient was calculated from the slope of mean squared displacements vs time (Fig. 1). A value of 9.35×10^{-5} cm^2/s was obtained for the translational diffusion coefficient for acetylene adsorbed in Na-Y zeolite. Information about the geometry of motion can be obtained from the intermediate scattering function which is the Fourier transform of $S(\boldsymbol{Q},\omega)$—the dynamic scattering function which in turn is proportional to the measured intensity in an inelastic neutron scattering experiment. ω is the angular frequency corresponding to energy transfer $\hbar\omega=E_i-E_f$ where E_i is the initial energy of the neutrons before scattering and E_f is the final energy of the neutrons after scattering. The intermediate scattering functions corresponding to translational motion of the molecules can be

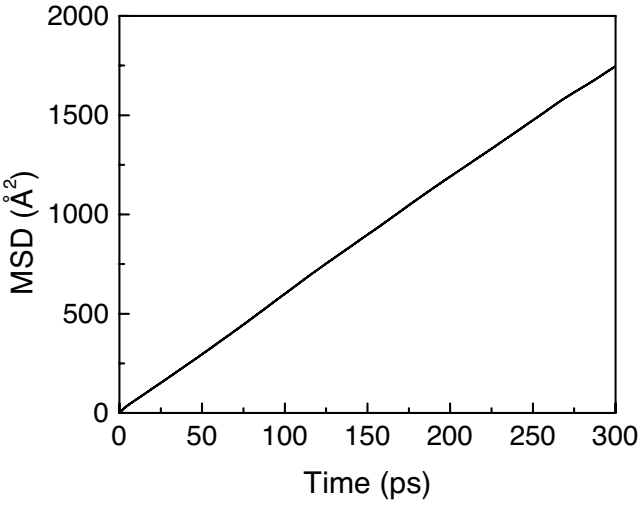

FIG. 1. Variation of mean square displacement with time.

calculated from the trajectories of center of mass obtained from the simulation and can be written

$$I(\mathbf{Q},t) = \langle\exp[i\mathbf{Q}\cdot(\mathbf{r}(t+t_0) - \mathbf{r}(t_0))]\rangle, \tag{3}$$

where $\mathbf{r}$ is the position vector of the center of mass of the scatterer and $\boldsymbol{Q}(=\mathbf{k}_i-\mathbf{k}_f$, where $\mathbf{k}_i$ and $\mathbf{k}_f$ are the wave vectors of neutron before and after scattering) is the wave vector transfer; the angular brackets indicate ensemble average. To calculate the powder averaged $I(Q,t)$ functions, an average over all $\boldsymbol{Q}$ vectors with a given magnitude has to be taken. This is useful to make comparison with the experimental data taken with the powder sample. Thus the powder averaged intermediate scattering function for translational motion can be written as,

$$I^{trans}(Q,t) = \overline{\langle\exp[i\mathbf{Q}\cdot\{\mathbf{r}(t+t_0) - \mathbf{r}(t_0)\}]\rangle}, \tag{4}$$

where bar denotes the average over all $\boldsymbol{Q}$ vectors with the same magnitude allowed by periodic boundary conditions.

The $I^{trans}(Q,t)$ functions calculated from the present MD simulation data and using Eq. (4) above were fitted using the following equation:

$$I^{trans}(Q,t) = A_1(Q)e^{[-t^2\Gamma_1^2(Q)/2]} + A_2(Q)e^{[-t\Gamma_2(Q)]} + A_3(Q)e^{[-t\Gamma_3(Q)]}. \tag{5}$$

Figure 2 shows the $I^{trans}(Q,t)$ functions as obtained from the MD simulation and the least squares fit using Eq. (5).

Generally, the intermediate scattering functions are expected to behave differently in two different regimes—(i) short time and small length scales and (ii) large time and long length scales. At very short time intervals, the particle sees no interactions and behaves like a free particle. The behavior of the intermediate scattering function for free particles (noninteracting and therefore behaving as a perfect gas) can be represented by a Gaussian function [15,25] as follows:

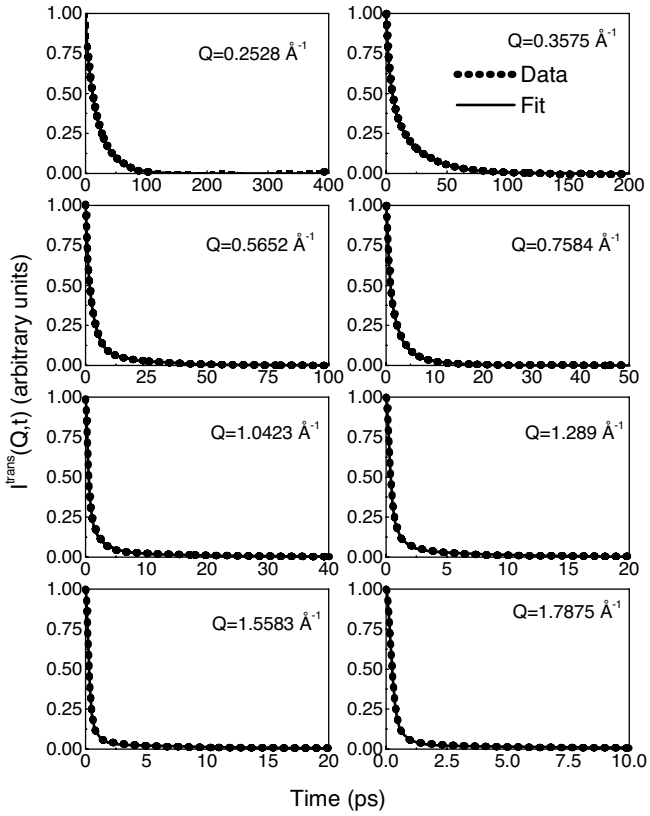

FIG. 2. The $I^{trans}(Q,t)$ vs t plots for the different Q values. The dotted line plot is the one obtained from the simulation whereas the solid curve is the fit with Eq. (5).

$$I(Q,t) = \exp\left(-\frac{Q^2t^2k_BT}{2m}\right). \tag{6}$$

Here, k_B and T are the Boltzman constant and temperature, respectively, and m is the mass of the particle.

Further, this Gaussian-like behavior of the intermediate scattering function becomes more pronounced at higher Q values since at small distances the particle also behaves as a noninteracting free particle. However, at large times and longer distances, the particle experiences several interactions and is no longer free. In the case of bulk liquid, the intermediate scattering function in this regime can be approximated by an exponential function. However, in the case of a porous medium, the motion of the particles and therefore the intermediate scattering function is expected to be influenced by its pore topology. In case of Na-Y zeolite, the pore topology consists of supercages and windows and this contributes to two distinct exponential functions corresponding to the motion of acetylene molecule within the supercages and window regions. Thus, in all, for a wide range of Q and t, the intermediate scattering function is approximated by a sum of a Gaussian and two exponentials. The behavior of respective weight factors (A_1, A_2, A_3) obtained from the least square fit of simulated $I^{trans}(Q,t)$ with Eq. (5) is shown in Fig. 3 as a function of Q. It can be seen from the plot that the weight factor for the Gaussian component, A_1 increases with increasing Q values. This suggests that as the Q value increases, the "free particle" regime is approached. As can be seen from Fig. 3, at small Q, the value of weight factor corresponding to one of the exponential functions (A_2) is small while the other one (A_3) is relatively large. At high Q values, both the exponential components will be small since at this length scale free particle type behavior dominates as discussed earlier.

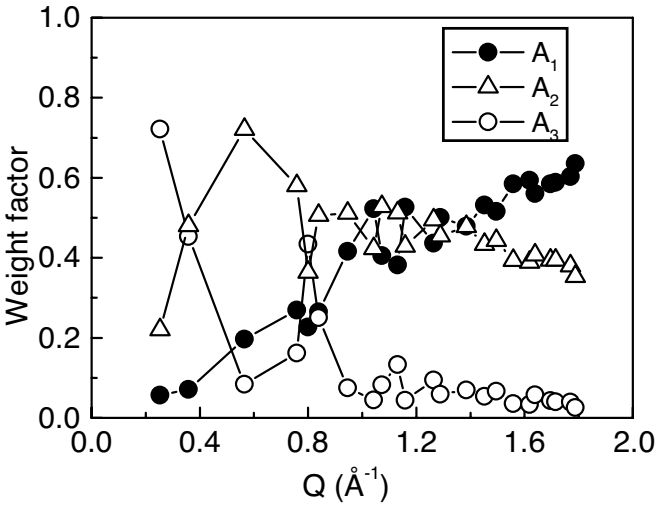

FIG. 3. The behavior of weight factors $A(Q)$ in Eq. (5) corresponding to the three components of the intermediate scattering function $I^{trans}(Q,t)$ with Q. Errors in the fitted weight factors are smaller than the size of the symbols.

The obtained values of $\Gamma_1(Q)$, $\Gamma_2(Q)$, and $\Gamma_3(Q)$ are in the range of ~0.7–3.4, ~0.1–1.7, and ~0.02–0.27 meV, respectively. Variations of these parameters with Q are shown in Fig. 4.

Comparing the first term in Eq. (5) with Eq. (6) one gets,

$$\Gamma_1(Q) = \sqrt{\frac{k_BT}{m}}Q. \tag{7}$$

Therefore, the variations of Γ_1 is linear with Q for a free particle dynamics. The solid line in Fig. 4 is the calculated line using Eq. (7) for acetylene molecule at 300 K.

A QENS experiment on acetylene in Na-Y zeolite performed using a QENS spectrometer that was designed to probe the dynamics at the energy scale of 0.2 meV has been reported earlier [17]. HWHM of quasielastic component is also plotted in Fig. 4. As it is evident from the figure, experimental width is closely following Γ_3 obtained from the simulation that is close to the energy scale of the experiment. The other two components are too fast to contribute to that QENS spectra and only Γ_3, corresponding to slowest motion contributed to the QENS spectra.

Trajectory of the center of mass of a single acetylene molecule over the entire period of simulation is shown in Fig. 5.

B. Rotational motion

Rotational motion in acetylene inside Na-Y zeolite cages is relatively faster and therefore the intermediate scattering functions for rotational motion decay much faster than that

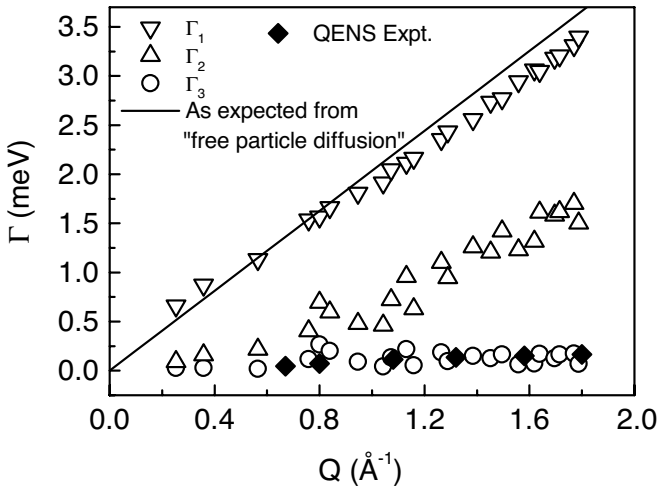

FIG. 4. The behavior of Γ values in Eq. (5) corresponding to the three components of the intermediate scattering function $I^{trans}(Q,t)$ with Q. Errors in the fitted Γ values are smaller than the size of the symbols. Filled diamond symbols show half width at half maximum (HWHM) of the quasielastic width obtained from the earlier experiment that was designed to probe dynamics at the energy scale of 0.2 meV. The line corresponds to the width as expected from free particle diffusion [Eq. (6)].

of translational motion. The rotational diffusion coefficient, D_R, can be obtained by integrating the angular velocity autocorrelation function (AVACF) defined

$$\mathrm{AVACF} = \langle \boldsymbol{\omega}_r(t+t_0)\boldsymbol{\omega}_r(t_0)\rangle, \tag{8}$$

where $\langle\rangle$ denotes the ensemble average and $\boldsymbol{\omega}_\mathbf{r}$ is the angular velocity. Therefore,

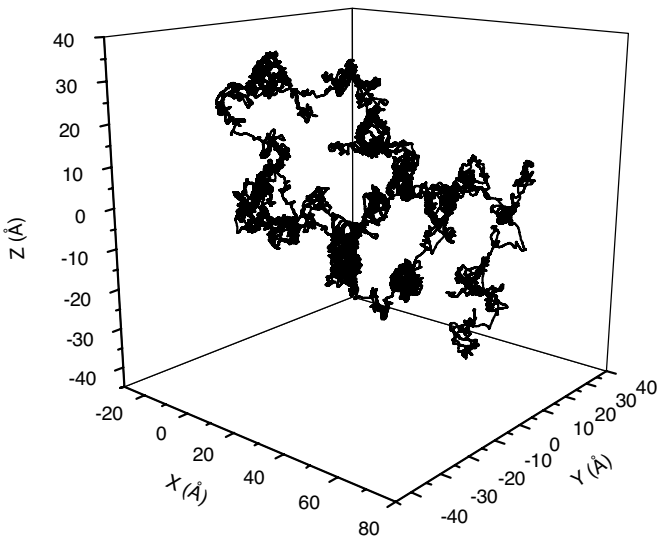

FIG. 5. The trajectory of the center of mass of an acetylene molecule saved from a production run of 1.3 ns. The particle starts its journey from the origin (0,0,0) at time $t=0$.

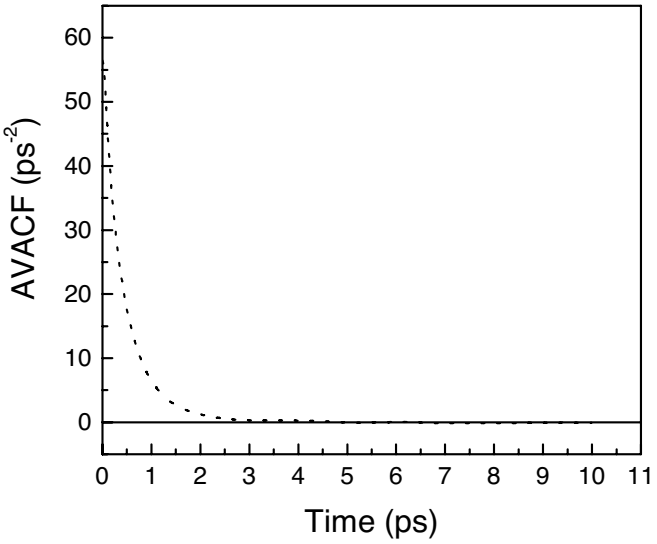

FIG. 6. Variation of angular velocity autocorrelation function with time.

$$D_R = \frac{1}{N_r}\int_0^\infty \langle \boldsymbol{\omega}_\mathbf{r}(t+t_0)\boldsymbol{\omega}_\mathbf{r}(t_0)\rangle dt, \tag{9}$$

where N_r is the number of degrees of freedom associated with rotational motion (for a linear molecule like acetylene, $N_r=2$). The angular velocity autocorrelation function calculated using Eq. (8) is shown in Fig. 6. Integration was carried out up to $t=50$ ps to take care of the possible long tail effect of the angular velocity autocorrelation function. For the present system a value of $\hbar D_R=8.5$ meV was obtained for the rotational diffusion coefficient for acetylene molecules. The intermediate scattering functions for rotational motion, $I^{rot}(Q,t)$ were calculated, as in the case of translational motion, for different Q values as follows:

$$I^{rot}(Q,t) = \overline{\langle \exp[i\mathbf{Q}\cdot\{\mathbf{d}(t+t_0)-\mathbf{d}(t_0)\}]\rangle}, \tag{10}$$

where $\mathbf{d}$ is the position vector of a CH site with respect to the center of mass of the acetylene molecule. $I^{rot}(Q,t)$ as calculated using Eq. (10) for some typical Q values are shown in Fig. 7.

In the QENS experiment, the most convenient way to extract the information about the rotational geometry is to analyze the behavior of the elastic incoherent structure factor (EISF), which is defined as the fraction of the elastic component to the total QENS spectra and can be given by

$$\mathrm{EISF} = \frac{I_{el}(Q)}{I_{el}(Q)+I_{qe}(Q)},$$

where $I_{el}(Q)$ and $I_{qe}(Q)$ are the elastic and quasielastic intensities, respectively. A plot of EISF vs Q can be compared with that predicted by various rotational diffusion models. In simulation, EISF can simply be found out as the value of $I^{rot}(Q,t)$ at long times. Therefore, EISF was obtained from different simulated $I^{rot}(Q,t)$ functions, as the value they take at long times. Figure 8 shows the variation of EISF obtained from the simulated $I^{rot}(Q,t)$ with Q. It is found that the iso-

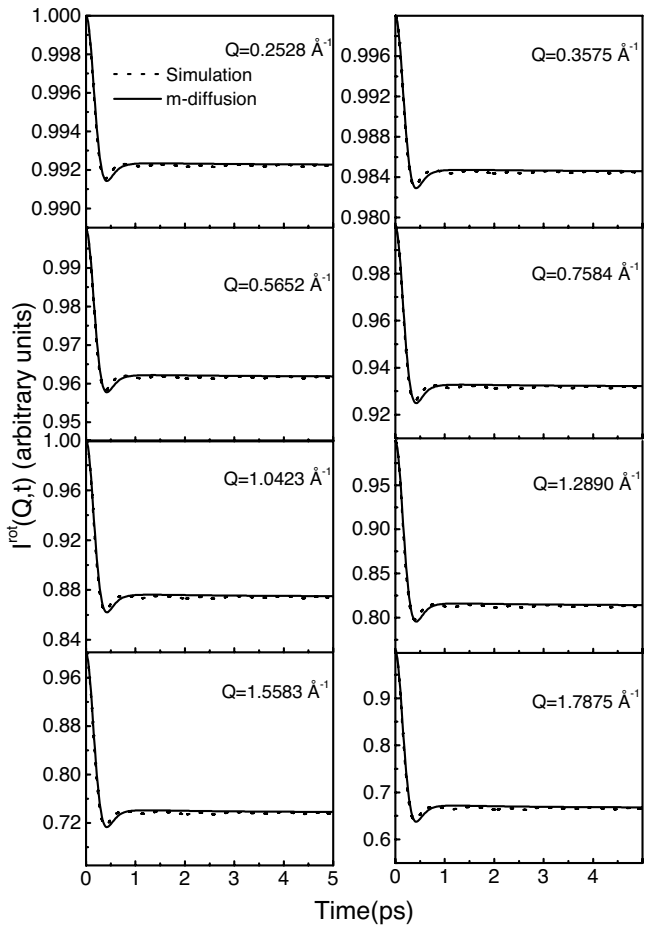

FIG. 7. The $I^{rot}(Q,t)$ vs t plots for the different Q values. The dotted lines are the ones obtained from the simulation whereas the solid curve is the fit with m-diffusion model.

tropic rotation model [as discussed later and in which EISF can be represented as $j_0^2(QR)$, where j_0 is spherical Bessel function of zeroth order and R is radius of rotation] fits the EISF quite well. This suggests that the rotational motion in acetylene molecules trapped in Na-Y zeolite cages is isotropic. The fit of EISF with the isotropic rotational model yielded a value for the radius of rotation of 0.6 Å. This is exactly the distance of one CH site from the center of mass.

In the isotropic rotational model, molecular reorientation is assumed to take place through random rotations in all directions. Then, on a time average, no most probable orientation exists. In an isotropic rotation, the rotational intermediate scattering function can be written in terms of the Legendre polynomials of time correlation functions of a unit vector fixed to the molecular axis [26]

$$I^{rot}(Q,t) = \sum_{l=0}^{\infty} (2l+1) j_l^2(QR) \langle P_l[\mathbf{u}(t)\cdot\mathbf{u}(0)]\rangle, \qquad (11)$$

where P_l is a Legendre polynomial of order l, R is the radius of rotation and $\mathbf{u}$ is a unit vector fixed to the molecular axis. The first term with $l=0$ will give the EISF which is independent of the behavior of Legendre polynomials since $P_0[\mathbf{u}(t)\cdot\mathbf{u}(0)]=1$. In the present case, R can be identified

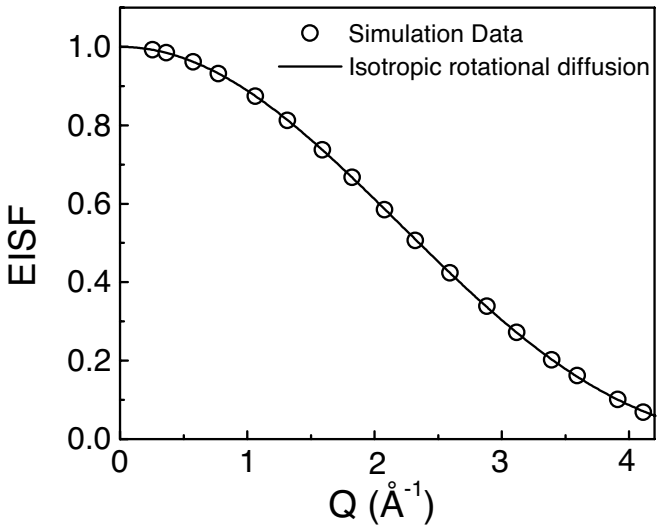

FIG. 8. Variation of EISF with Q. Open circles show the simulation data points whereas the solid curve is the fit with isotropic rotational diffusion model.

with d, the distance of one CH site from center of mass of the acetylene molecule. An average is taken over all initial times $t=0$. A detailed analysis of rotational correlations required considerations beyond EISF as discussed below.

1. Rotation through small angles

Assuming isotropic rotational diffusion comprising random small angle jumps in all directions, the expression for the intermediate scattering functions can be obtained from Eq. (11) by putting the Legendre polynomials as [26]

$$\langle P_l[\mathbf{u}(t)\cdot\mathbf{u}(0)]\rangle = \exp[-l(l+1)D_R t], \qquad (12)$$

where D_R is the rotational diffusion coefficient.

The $I^{rot}(Q,t)$ functions calculated using simulation data show a dip (Fig. 7), which could not be fitted with a function having monotonic decay as in the small angle isotropic diffusion [Eq. (12)]. These functions were therefore fitted with another isotropic rotation model—the m-diffusion model as described below.

2. Rotation through large angles (m-diffusion model)

This is an isotropic rotational model where large rotational jumps are included. It was found that for small molecules, the random rotations are not restricted to small angles only [27,28]. Gordon suggested a model [29] involving rotational jumps of arbitrarily large angles where the direction of the angular momentum vector $\mathbf{J}$ changes but its magnitude remains the same. Since this rotational motion is also isotropic in nature the intermediate scattering function is again given by Eq. (11). However, the behavior of the Legendre polynomials here are different from those in the case of small angle rotational diffusion. As shown by Barojas and Levesque [30], the average of Legendre polynomials for m diffusion can be calculated as follows:

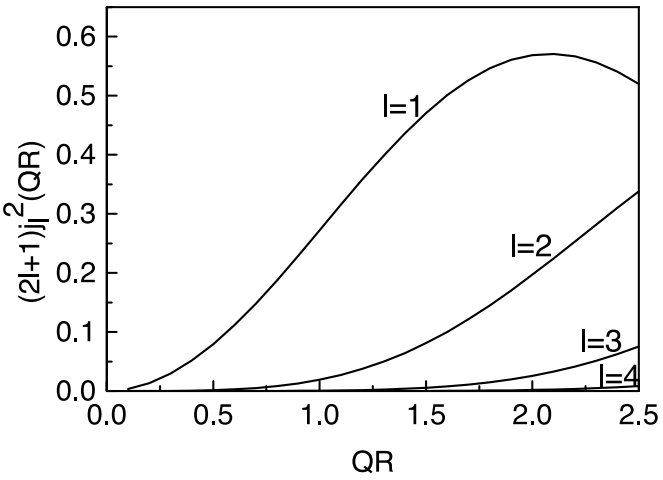

FIG. 9. The first four Bessel functions that have significant values up to $QR=2.5$.

$$\langle P_l[\mathbf{u}(t)\cdot\mathbf{u}(0)]\rangle = e^{-t/\tau}\int_0^\infty \omega_r e^{-\omega_r^2/2} G_M^l(t)d\omega_r, \qquad (13)$$

where τ is the time spent by the molecule between two successive collisions, ω_r is the angular velocity of rotational motion, and

$$G_M^l(t) = \sum_{n=0}^{\infty}\frac{1}{\tau^n}\int_0^t dt_n f_M^l(t-t_n), \quad \int_0^{t_n} dt_{n-1} f_M^l(t_n - t_{n-1})\cdots,$$
$$\times\int_0^{t_2} dt_1 f_M^l(t_2-t_1) f_M^l(t_1). \qquad (14)$$

Here,

$$f_M^l(t) = P_l(\omega_r t).$$

Equation (14) is equivalent to the Volterra equation

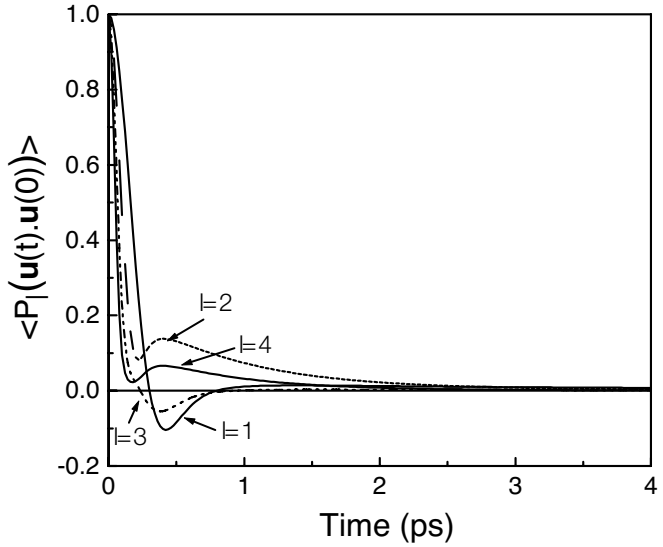

FIG. 10. The first four Legendre polynomials calculated for *m*-diffusion in acetylene molecules adsorbed in Na-Y zeolite.

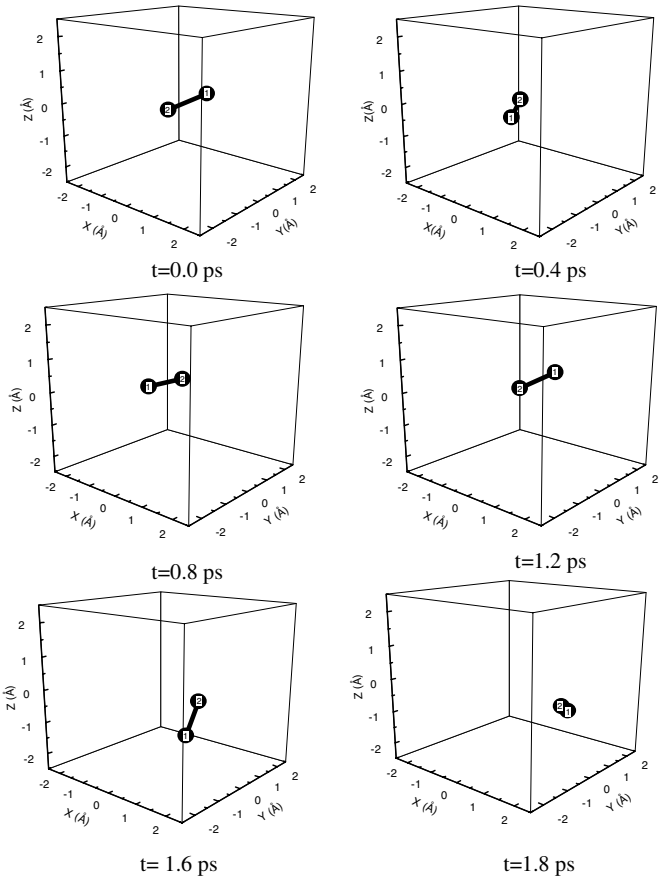

FIG. 11. Snapshots from molecular dynamics to show the translational and rotational motion. The two CH sites are numbered in order to distinguish them from each other. The acetylene molecule is shown to be moving in a cubic box of size 5 Å.

$$G_M^l(t) = f_M^l(t) + (1/\tau)\int_0^t f_M^l(t-s)G_M^l(s)ds. \qquad (15)$$

This equation can be solved numerically [31]. It is seen that with $Q_{max}R$ equal to 2.43, structure factor $(2l+1)j_l^2(QR)$ has a significant contribution only up to $l=4$ as seen from the plot of $(2l+1)j_l^2(QR)$ vs QR for different values of l (Fig. 9). The Legendre polynomials of different order (up to $l=4$) were calculated using simulation data. Simulated Legendre polynomials are shown in Fig. 10. The first order Legendre polynomial can be written

$$\langle P_1[\mathbf{u}(t)\cdot\mathbf{u}(0)]\rangle = \langle \mathbf{u}(t)\cdot\mathbf{u}(0)\rangle. \qquad (16)$$

This is a dipole correlation function. As can be seen in Fig. 10, this function goes to negative, suggesting that it is more probable to find a dipole in the hemisphere opposite to that in which it began at a time t earlier. In other words the molecule has turned through a large angle. This confirms the occurrence of large angular jumps in the case of the rotation of acetylene.

$I^{rot}(Q,t)$ were then fitted with the *m*-diffusion model with τ as a parameter. While fitting $I^{rot}(Q,t)$ with Eqs. (11) and (13), up to $l=4$ terms are found sufficient to be considered in

the expansion. Equation (13) was integrated up to a $\omega_r = 10$ ps^{-1}. A value of $\tau = 0.55$ ps gave the best fit to $I^{rot}(Q,t)$ functions. It can be seen from Fig. 9 that the contribution from the first order Legendre polynomial is dominant. This mainly gives rise to the unusual dip in the $I^{rot}(Q,t)$ functions. The $I^{rot}(Q,t)$ functions fit well with the *m*-diffusion model as shown in Fig. 7.

MD snapshots of a single acetylene molecule in a cubic box of side 5 Å are shown in Fig. 11.

IV. CONCLUSIONS

We have carried out molecular dynamics simulation studies of acetylene molecules adsorbed in Na-Y zeolite. From the MD simulation, it was observed that the translational motion in acetylene molecules adsorbed in Na-Y zeolite occurs at three different time scales. At short time and small length scales, acetylene molecules perform free particle motion inside Na-Y zeolite whereas at longer time and larger length scales the center of mass motion is found to be dependent on the pore topology. Translational motion corresponding to slowest motion contributes to the quasielastic neutron scattering experiment performed earlier. It has been observed that the rotational motion in acetylene adsorbed in Na-Y zeolite is very fast. This might be attributed to the small moment of inertia of the acetylene molecules. The rotational motion of acetylene adsorbed in Na-Y zeolite cages has been found to occur through large angle jumps between successive steps during which the magnitude of the angular momentum remains conserved as in the *m*-diffusion model of rotational motion. Diffusion coefficients have been obtained using correlation functions in the case of translational as well as rotational motion.

[1] G. Tomlinson, *Modern Zeolites, Structure and Function in Detergents and Petrochemicals* (Traw Tech Publications Ltd., Switzerland, 1998).

[2] *Studies in Surface Science and Catalysis 58: Introduction to Zeolite Science and Practice*, edited by H. van Bekkum, E. M. Flanigen, and J. C. Jansen (Elsevier, Amsterdam, 1991).

[3] A. K. Tripathi, A. Sahasrabudhe, S. Mitra, R. Mukhopadhyay, and N. M. Gupta, Phys. Chem. Chem. Phys. **3**, 4449 (2001).

[4] A. Sahasrabudhe, S. Mitra, A. K. Tripathi, R. Mukhopadhyay, and N. M. Gupta, J. Phys. Chem. B **106**, 10923 (2002).

[5] S. Mitra, R. Mukhopadhyay, A. K. Tripathi, and N. M. Gupta, Appl. Phys. A **74**, S1308 (2002).

[6] A. Sahasrabudhe, S. Mitra, A. K. Tripathi, R. Mukhopadhyay, and N. M. Gupta, Phys. Chem. Chem. Phys. **5**, 3066 (2003).

[7] A. Sayeed, S. Mitra, A. V. Anil Kumar, R. Mukhopadhyay S. Yashonath, and S. L. Chaplot, J. Phys. Chem. B **107**, 527 (2003).

[8] R. Mukhopadhyay, A. Sayeed, S. Mitra, A. V. Anil Kumar, M. N. Rao, S. Yashonath, and S. L. Chaplot, Phys. Rev. E **66**, 061201 (2002).

[9] P. K. Ghorai, S. Yashonath, P. Demontis, and G. B. Suffritti, J. Am. Chem. Soc. **125**, 7116 (2003).

[10] J. Kärger and D. M. Ruthven, *Diffusion in Zeolites and Other Microporous Solids* (Wiley-Interscience, New York, 1992).

[11] J. Caro, M. Bulow, W. Schiner, J. Kärger, W. Heink, H. Pfeifer, and S. P. Zdanov, J. Chem. Soc., Faraday Trans. 1 **81**, 2541 (1985).

[12] M. Bee, *Quasielastic Neutron Scattering* (Adam Hilger, Bristol, 1988).

[13] S. Mitra and R. Mukhopadhyay, Curr. Sci. **84**, 653 (2003).

[14] M. P. Allen and D. J. Tildesley, *Computer Simulation Of Liquids* (Oxford University Press, Oxford, 1987).

[15] F. R. Trouw, Spectrochim. Acta, Part A **48A**, 455 (1992).

[16] P. L. Hall and D. K. Ross, Mol. Phys. **42**, 673 (1981).

[17] S. Mitra and R. Mukhopadhyay, Pramana-J. Phys. **63**, 81 (2004).

[18] A. N. Fitch, H. Jobic, and A. Renouprez, J. Phys. Chem. **90**, 1311 (1986).

[19] S. Calero, D. Dubbeldam, R. Krishna, B. Smit, T. J. H. Vlugt, J. F. M. Denayer, J. A. Martens, and T. L. M. Maesen, J. Am. Chem. Soc. **126**, 11377 (2004).

[20] E. Dubbeldam, E. Beerdsen, T. J. H. Vlugt, and B. Smit, J. Chem. Phys. **122**, 224712 (2005).

[21] H. Jobic, J. Mol. Catal. A: Chem., **158**, 135 (2000).

[22] H. Jobic, J. Kärger, and M. Bee, Phys. Rev. Lett. **82**, 4260 (1999).

[23] S. Yashonath, J. M. Thomas, A. K. Nowak, and A. K. Cheetham, Nature (London) **331**, 601 (1988).

[24] W. L. Jorgensen, J. D. Madura, and C. J. Swenson, J. Am. Chem. Soc. **106**, 6638 (1984).

[25] P. A. Egelstaff, *An Introduction to the Liquid State* (Academic Press, London, 1967).

[26] V. F. Sears, Can. J. Phys. **44**, 1279 (1966).

[27] R. G. Gordon, J. Chem. Phys. **42**, 3658 (1965).

[28] R. G. Gordon, J. Chem. Phys. **43**, 1307 (1965).

[29] R. G. Gordon, J. Chem. Phys. **44**, 1830 (1966).

[30] J. Barojas and D. Levesque, Phys. Rev. A **7**, 1092 (1973).

[31] W. Press, S. A. Teukolsky, W. T. Vetterjing, and B. P. Flannery, *Numerical Recipes in Fortran* 2nd edition (Cambridge University Press, Cambridge, 1986).